Eco-friendly and Cost-Effective Synthesis of Lead Sulfide Nanocrystals Attached to Nitrogen-doped Carbon Nanotubes

B. Rebollo-Plata[1], M. P. Sampedro[2], M. López-Fuentes[3], J. G. Cabal-Velarde[1], M. Guzmán-Altamirano[1], O. Portillo-Moreno[4], A. Lobo-Guerrero[5], G. Gómez-Espinoza[6] and Raúl A. Morales-Luckie[7]

[1]Tecnológico Nacional de México-Instituto Tecnológico Superior de Irapuato, Km 12.5 Carr. Irapuato-Silao, Guanajuato, 36821, México.

[2]Facultad de ingeniería Química BUAP, Av. San Claudio y 18 Sur, Col. San Manuel, C.P. 72570 Ciudad Universitaria Puebla, Pue. México.

[3]Complejo Regional Centro, BUAP, Carretera Castañeda Morelos Km 7.5, El Salado, C.P. 75460, Tecamachalco, Puebla, México.

[4]Laboratorio de Materiales Sci., Facultad de Ciencias Químicas, Benemérita Universidad Autónoma de Puebla, Av. San Claudio y 18 Sur, 72570, Puebla, México.

[5]Área Académica de Ciencias de la Tierra y Materiales, Universidad Autónoma del Estado de Hidalgo, Carr. Pachuca-Tulancingo km 4.5, 42039, Mineral de la Reforma, México.

[6]Departamento de Ingeniería Agroindustrial, Universidad Politécnica de Pénjamo, Carr. Irapuato- La Piedad km 44, Predio El derramadero, Pénjamo, Guanajuato, 36921, México.

[7]Centro Conjunto de Investigación en Química Sustentable UAEM-UNAM, Carretera Toluca-Atlacomulco Km 14.5, San Cayetano, Toluca C.P. 50200, México

Corresponding author: M. P. Sampedro, E-mail: mpstraviata@hotmail.com, cell phone: (52)2221474970

The research is financed by: The authors

Abstract:

Lead sulfide (PbS) nanocrystals anchored on nitrogen-doped multiwalled carbon nanotubes (N-CNTs) are synthesized employing an environmentally friendly and inexpensive wet chemistry process. PbS/N-CNTs composites are examined by scanning electron microscopy, X-ray diffraction, Raman spectroscopy, and *ab initio* theoretical calculations to determine their morphological, optical, and structural properties. The PbS nanoparticles exhibit a 15 nm particle size with a face-centered cubic crystal structure and are homogeneously distributed along the carbon nanotubes. Nitrogen doping on CNTs acts as binding sites for the PbS clusters as *Ab initio* theoretical study suggests.

Keywords*:* Lead Sulfide; Carbon Nanotubes; Nanoparticles; Nitrogen-doping; density functional theory.

1. Introduction

Nanometer-size sp2 carbon-based materials findings, such as graphene, fullerenes, and carbon nanotubes (CNTs) have led to a vast number of reports in this field. Graphene carbon atoms are densely organized in a regular sp2 honeycomb configuration, which is the basic pattern for other sp2 carbon allotropes such as fullerenes, nanoribbons, and CNTs. CNTs possess unique electronic, optical, and structure properties, suitable for use as a substrate for a wide range of nanoparticles [1-9]. Nitrogen-doped CNTs (N-CNTs) have been the preferred microstructure for nanoparticle enrichment mechanism due to their distinct morphology (e.g., large defect density) and chemical properties [1-5]. In this way, semiconductor nanocrystals attached to N-CNTs have been used to produce solid-state composites for diverse applications [10,11].

On the other hand, Lead sulfide (PbS) nanocrystals have a relatively small bandgap (Eg ~0.41 eV at 300 K), and they have applications in a great variety of technological and optoelectronic construction devices due to their high third-order nonlinear optical properties [12]. PbS grain size and bandgap (Eg) are easily adjustable by systematic doping with trivalent ions [13], making optical, morphological, structural, and electronic properties possible to be modulated. Strong quantum effects are observed at ~30 nm particle sizes where material properties are significantly affected and open the opportunity to design a new generation of optoelectronic devices. In this context, PbS/N-CNTs composite synthesized with different techniques among which the electrostatic interaction, ultrasound-assisted, and chemical methods highlight allow fabricating different architectures, such as high-performance photo-switches, field emission devices, quantum dot sensitized solar cells, and supercapacitors [14-17]. This report addresses a green, versatile, and cost-effective procedure to anchor PbS nanocrystal onto the surface of N-CNTs efficiently. The PbS/N-CNTs composite is examined by scanning electron microscopy, X-ray diffraction, FT-IR, and Raman spectroscopy. Ab initio simulations helped to identify the possible anchoring sites.

Graphite possesses a double resonant scattering process closely related to those in carbon nanotubes. Raman spectra has been calculated with D mode using the concept of double resonances. Dependence on excitation energy is the main reason why re-examining the D mode, which stills un-solve to these days. In the high energy part, the peak labeled D is a defect-induced mode [18-20]. In this work, the peak D is in the position $\sim 1326\ cm^{-1}$.

2. Materials and methods

2.1. Material synthesis

The PbS nanocrystals growth was carried out by mixing $Pb(CH_3COO)_2$, KOH, and NH_4NO_3. This reaction takes place predominantly over the direct hydrolysis of thiourea in the bulk of the chemical bath [21,22].

$$SC(NH_2)_2 + 3OH^- \Leftrightarrow CO_3^{2-} + HS^- + 6H^+ \qquad (1)$$

$$Pb(CH_3COO)_2 \Leftrightarrow 2CH_3COO^- + Pb^{2+} \qquad (2)$$

The complex ion formed in our working conditions generates the slow release of ions Pb^{2+}

1. $$[Pb(NH_3)_4]^{2+} + S^{2-} \Leftrightarrow PbS + 4NH_3 + 2H^+ \qquad (3)$$

This reaction described in (3) is not spontaneous since its free energy change (ΔG^0 = +362.88 KJ) is positive. The nanocrystals were then washed with abundant deionized water and dried at room temperature. The process was repeated several times until the largest amount of contaminated waste was removed. The solutions for the PbS growth were the followings: $Pb(CH_3COO)_2$ (0.01 M), KOH (0.5 M), NH_4NO_3 (1.5 M), $SC(NH_2)_2$ (0.2 M). All the solutions used were prepared with deionized water with 18.2 MΩ[12].

The N-CNTs were synthesized by chemical vapor deposition (CVD) using the experimental set-up described in other previously reported articles [23-25]. Briefly, a solution containing ferrocene [$Fe(C_5H_5)_2$] (2.5 wt %) dissolved in benzylamine ($PhCH_2NH_2$) was pyrolyzed for 20 min using a two-stage furnace system at 800 ^{0}C with an argon gas flow rate of 2.5 L/min. The N-CNTs then are collected from the soot deposited on the quartz tube located inside the furnace.

Produced PbS/N-CNT composite was dispersed ultrasonically (GEX130 equipment), for 1 hour in acetone at room temperature, we used different weights of nanotube powders and PbS powder in acetone (ratio PbS/N-CNTs = 0.2, 0.1, 0.098, 0.096, 0.06 and 0.02) reaching an optimal architecture in the N-CNTs/PbS grain ratio of 0.02 um.

Characterization: The samples were characterized by scanning electron microscopy (SEM) using a QUANTA 200 3D, FEI microscope, operating at 20 kV and equipped with energy-dispersive X-ray spectroscopy for obtaining superficial micrographs along with basic chemical analysis (EDS). X-Ray analysis was performed by using a Brucker diffractometer; Raman spectroscopy was carried out in a Lab Raman, Dillor ($\lambda = 514\ and\ 633\ nm$) apparatus, and Fourier transforms infrared spectra (FT-IR) were recorded in a Perkin-Elmer spectrophotometer.

2.2. Computational details

Density functional theory (DFT) and the generalized gradient approximation with the revised Perdew, Burke, and Ernzerhof (RPBE) approach as the exchange-correlation term [26] performed the calculations method. Linear combination of pseudo-atomic numerical orbitals using double-ζ plus one polarized orbital basis [27] represented wave functions for the valence electrons. A 1×1×10 Monkhorst-Pack grid was used to sample the 1D Brillouin zone. A Methfessel-Paxton smearing of 25 meV and a Pulay mixing is employed to aid convergence on the self-consistent electron density. The real-space grid used for charge and potential integration is equivalent to a plane wave cut-off energy of 400 Ry. 12-unit cell of a metallic (6,6) single-walled carbon nanotube (SWCNT) simulated the CNTs with a total of 288 atoms.

The DFT calculations were performed using the SIESTA code [28]. The interaction strength between the PbS cluster and SWCNTs was evaluated by calculating the adsorption energy (ΔE_{ads}) defined as: $\Delta E_{ads} = E_{tot} - E_{Sub} - E_{NPs}$, where E_{tot} is the total energy of the $Pb_{18}S_{18}$-SWCNTs system and E_{Sub} (E_{NPs}) is the energy of the substrate (PbS nanocrystal). The Voronoi charge analysis was used to determine the transferred electronic charge among the components using the optimized geometries and 400 Ry as energy cut-off for the real-space grid [29]. The 3D representation of charge transfer $\delta n(r)$ of the $Pb_{18}S_{18}$-SWCNTs systems was obtained by subtracting the charge densities of the nanotubes ($n(r)_{CNT}$) and $Pb_{18}S_{18}$ ($n(r)_{PbS}$) from the total charge density of the $Pb_{18}S_{18}$-SWCNT system ($n(r)_{total}$). The charge transfer is given by $\delta n(r) = n(r)_{total} - n(r)_{CNT} - n(r)_{PbS}$.

The N-CNT was simulated by introducing diverse substitutional and pyridine-like nitrogen along with the (6,6)-SWCNT structure resulting in 6.0% N concentration. The PbS nanocrystal was constructed from the FCC bulk crystal structure, where a $Pb_{18}S_{18}$ symmetric cluster is obtained and then geometrically optimized before any adsorption event. The adsorption processes were performed by placing the $Pb_{18}S_{18}$ at 2.5 Å above SWCNTs. The periodically repeated systems are separated by at least

30 Å of vacuum to avoid lateral interactions. All systems could relax freely until the residual forces were < 0.04 eV/Å.

3. Results and discussion

3.1 Material characterization

N-CNTs decorated with PbS nanocrystals are shown in Figure 1 where the composite exhibits a homogeneous distribution of PbS crystals along the surface of the nanotubes. The PbS nanocrystals exhibit a particle size of 15 nm, like previous reports [30]. X-ray powder diffraction (XRD) of the PbS/N-CNTs composite is shown in Figure 2. The crystalline planes show a widening, which is closely related to the existence of the nanocrystals. Therefore, the incorporation of PbS nanocrystals onto N-CNTs is confirmed. The N-CNTs reflections have been reported, although they exhibit an amorphous behavior [31,32]. The XRD patterns showed reflections at 25.9°, 29.1°, 43.1°, 48.0° 51.0°, and 61.8°, which are associated with the (111), (100), (220), (311), (400) crystalline planes of the PbS nanocrystals, consistent with a face-centered cubic (FCC) crystal phase. These results agree with others already reported. The reflections at 29.3° and 48.2° correspond to the N-CNTs (labeled with an asterisk). It is worth mentioning that the reflectance intensity at 61.8°represents a preferred orientation in this crystalline plane, and such behavior has not been observed previously [12-13,33].

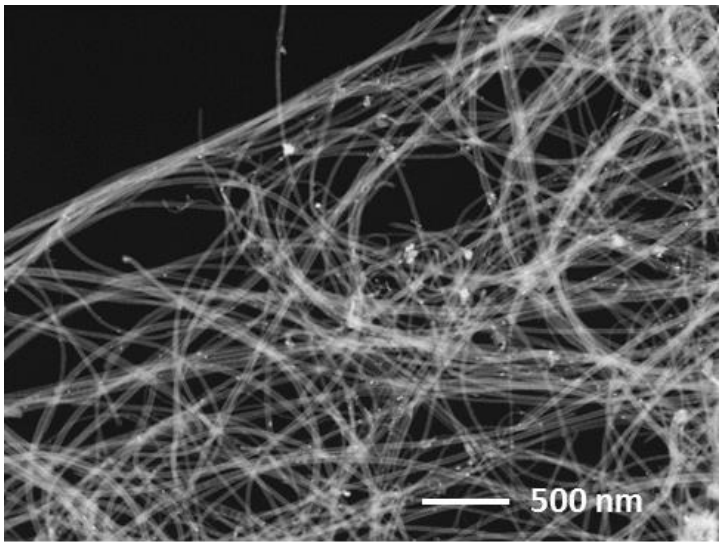

Figure 1. N-CNTs SEM micrograph with PbS nanoparticles anchored uniformly on the surface.

Figure 3 depicts the Raman spectra of the PbS nanocrystal anchored on N-CNTs. Some typical vibrational modes of carbon nanotubes are at 1325.85 and 1585.96 cm^{-1}, corresponding to the D and G bands [34,35]. Unfortunately, it is not possible to show the effect of nitrogen doping since it appears at low frequencies [31]. The vibrational modes at 139.93, 199.02, 429.14, and 967.12 cm^{-1} are assigned to the fundamental longitudinal optical (LO) phonon mode of rock-salt structure, first overtone (2LO) and second overtone (3LO) of PbS nanocrystal, respectively [13,21].

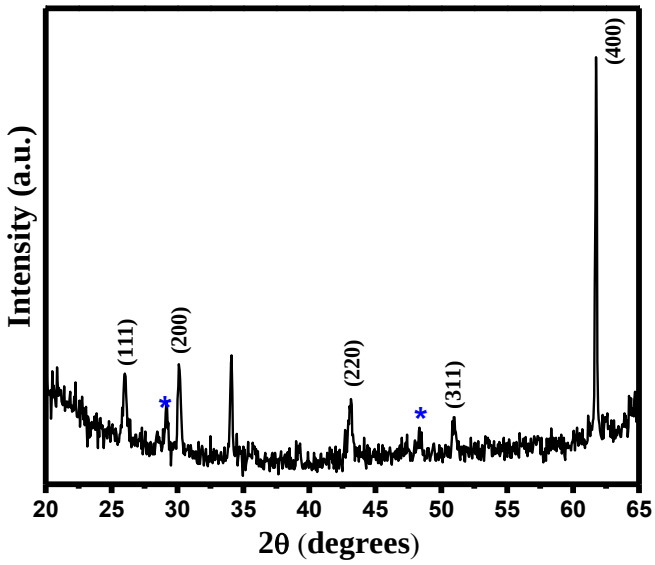

Figure 2. X-ray diffractogram of N-CNTs decorated with PbS nanocrystals.

Raman spectra band located at 140 cm-1 is attributed to a combination of longitudinal and transversal acoustic modes. The band centered at 967 cm-1 could be due to sulfates presence in the sample, instead of PbS laser-induced degradation, which is usually produced by the intensity of the laser oxidizing sulfates [36], or by the influence of the substrate [37] as reported in other works. However, the position and intensities of Raman peaks are also influenced by differences in particle sizes and the atomic composition effect. The G band in graphite involves an optical phonon mode between the two dissimilar carbon atoms in the cell unit. The corresponding mode in SWNT carries the same name.

The graphite Raman G band exhibits one single Lorentzian peak at $1582\ cm^{-1}$ related to the tangential mode vibrations of the C atoms. the SWNT G band is composed of several peaks due to the phonon wave vector confinement along the SWNT circumferential direction and due to symmetry-breaking effects associated with SWN curvature [20]. The dominant feature in the second-order Raman spectra in graphite and SWNTs is the G' band, which features from a two-phonon intervalley in a second-order Raman scattering process. For a high-quality sample, G' spectra are completely free from defect contributions, and the experimental G' band signal can be comparable in intensity to G band signal. The Raman spectra for the G' band phonon energy region have been calculated in the context of a double resonance process and considering both electron-photon and electron-phonon coupling for two phonon-emitting processes [20,38].

In general, the Raman spectra showed two major peaks of D and G bands appearing at around 1340 and $1580\ cm^{-1}$, deriving from the in-plane motion of the carbon atoms to provide a signature of carbon nanotubes. The Raman spectra feature of nitrogen carbon nanotubes has two major peaks at 1326 and $1584\ cm^{-1}$. Reported that the Raman spectra signal of carbon nanotubes is susceptible to strain effects and doping. The shift of the bands is due to the doping effect of the nitrogen. The obtained features of the nitrogen-doped carbon nanotubes Raman spectra are attributable to the multi walls of the nanotubes because of the absence of the radial breathing mode (RBM) to be observed, which normally appears between 120 and $250\ cm^{-1}$ in a single-wall nanotube [39-40]. Furthermore, it is mentioned that the G and P bands are attributed to the carbon-based materials sp^2 hybrid sites.

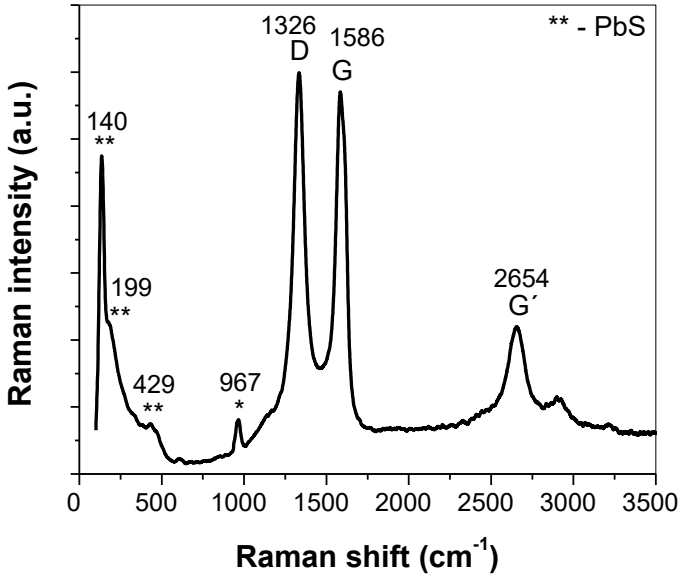

Figure 3. Raman spectra of PbS nanoparticles anchored on N-CNTs. The D, G and G´ bands correspond to N-CNTs. Peaks marked by (**) are attributed to PbS, and those with (*) to residual sulfates.

Finally, by analyzing the FT-IR spectra, the vibration and stretching bands of this material were identified. Figure 4 shows the FT-IR spectrum of PbS nanocrystals anchored on N-CNTs. The absorption bands attributed to the vibrations of CO_3^{2-}anions are located within the 3600-400 cm^{-1} region; see eq. (1). The peaks located at 1377 and 838 cm^{-1} are characteristic vibration bands of CO_3^{2-}ions. The sharp absorption band at 838 cm^{-1} was assigned to the bending out-plane vibrations. The broad absorption band in the 3385-3304 cm^{-1} region is due to st vibrations of -OH groups [41].

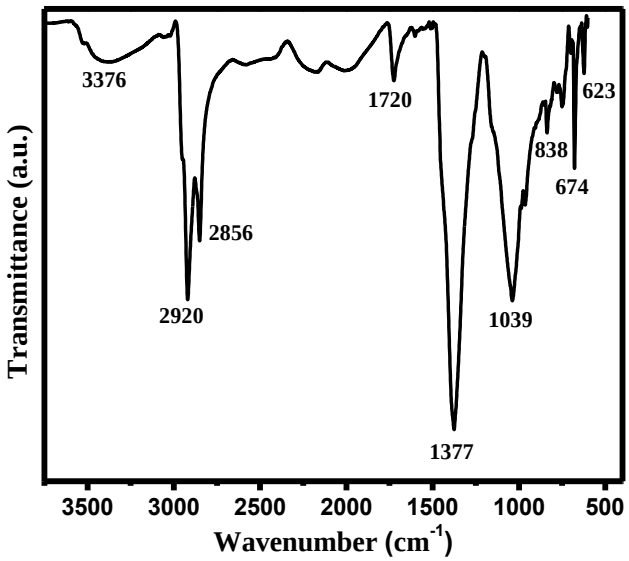

Figure 4. FT-IR spectrum of PbS/N-CNTs composites.

Furthermore, two peaks located at 2920 and 2856 cm^{-1} are related with $-CH_2$ group in the asymmetric stretching vibration and symmetric stretching vibration, respectively, see eq. (2). The band located at 1720 and 1377 cm^{-1} were assigned to the stretching vibration of $–C-OO^-$ ion and the -C-H vibration. Finally, the two peaks located at 674 and 623 cm^{-1}were attributed to the -C-S stretching and the S-S vibration modes [42].

3.2 Theoretical description of the PbS/N-CNTs composite

PbS nanoparticles interaction onto N-CNTs was examined by *ab initio* theoretical calculations to elucidate the nature of the interaction between these systems. N-doped (6,6) single-walled carbon nanotubes (SWCNT) substrate materials contain substitutional and pyridine-like nitrogen along their surface in 6% of N concentration. The introduction of diverse heteroatoms into CNTs structure is a widely used technique to enhance chemical reactivity. As a result, the electronic and chemical properties are significantly altered compared to the pristine (6,6)-SWCNT. By comparing the density of states (DOS), the introduction of localized states around the Fermi level generated by the pyridine-like N can be observed in Figure 5 where the N-doped sites act as preferential adsorption sites for different gases and nanoparticles. Here, the pyridine-like site was considered the anchoring site for the PbS nanocrystal (indicated by a dashed circle).

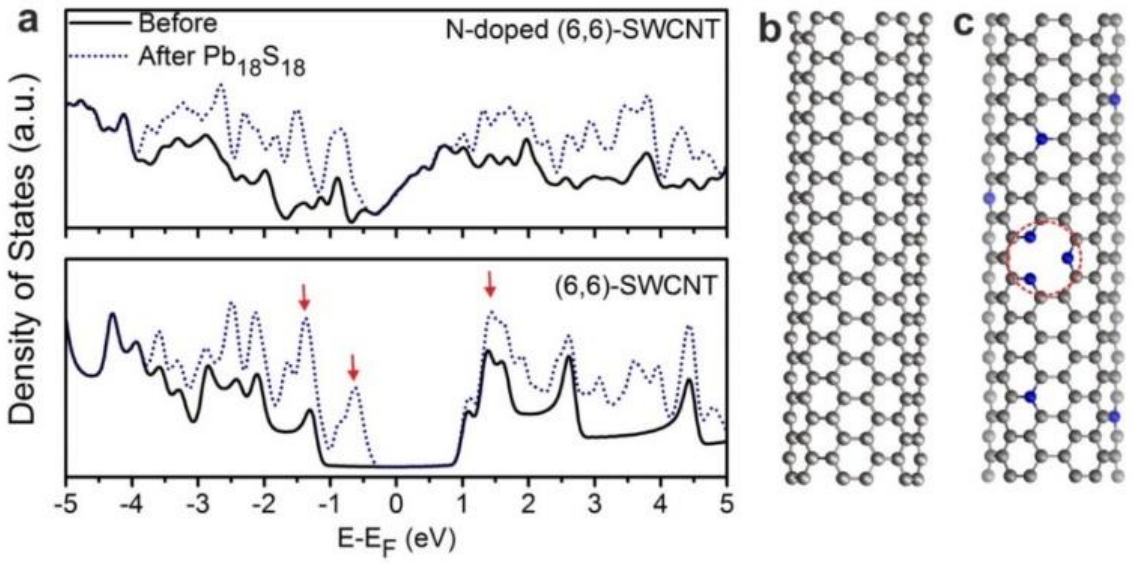

Figure 5. (a) Density of states (DOS) of (6,6)-SWCNT (bottom) and N-doped (6,6) SWCNT (top), before (solid line) and after (dashed line) the adsorption of the $Pb_{18}S_{18}$ cluster. (b-c) Optimized structure of pristine and N-doped (6,6) SWCNT. The dashed circle in (c) indicates the adsorption site. Gray (blue) spheres represent carbon (nitrogen) atoms.

The composite was constructed placing a symmetric $Pb_{18}S_{18}$ cluster at 2.5 Å above the SWCNTs, both pristine and N-doped. The optimized structures are depicted in Figure 6. After the adsorption process, $Pb_{18}S_{18}$ clusters do not modify their structure considerably, which may suggest a poor interaction, especially on the pristine (6,6)-SWCNT (Figure 6(a-b)). However, a detailed analysis showed that in the case N-doped (6,6)-SWCNT, a Pb atom at the interface is slightly pulled towards the pyridine-like defect suggesting a stronger interaction. In order to support this statement, the adsorption energy (ΔE_{ads}) of the $Pb_{18}S_{18}$ cluster was calculated, and it is found that the ΔE_{ads} on N-SWCNT systems is equal to -1.45 eV (negative values indicate an enhanced interaction), compared with -1.12 eV when pristine (6,6)-SWCNT is used.

Besides, the chemical bond nature was studied by calculating the electronic charge transfer between the $Pb_{18}S_{18}$ cluster and the SWCNTs. A Voronoi-type analysis indicated that the $Pb_{18}S_{18}$ cluster has a negative net charge and, in the case of N-doped SWCNT substrate, 0.3 e^- are transferred from the nanotubes to the $Pb_{18}S_{18}$ cluster. On the other hand, just0.2 e^- are transferred to the cluster when the pristine nanotubes are used. These results are consistent with the calculated ΔE_{ads} and indicate that N-doped SWCNT is better support material. The charge transfer between the $Pb_{18}S_{18}$ cluster and SWCNTs is also plotted in Figure 6 The black iso-surfaces indicate regions where there is an increase in electronic charge after the adsorption process, while white iso-surfaces indicate areas with depletion of charge density.

From Figure 6(c-d), it is possible to observe that when the N-doped SWCNT is used, a larger amount of e^- are transferred (in agreement with the Voronoi analysis), where the pyridine-like defect and one of the Pb atoms are the components that contribute most to the interaction. However, in the case of pristine (6,6)-SWCNT, the S atoms are the main responsible for the bonding, as observed from Figure 6(a-b), where S atoms exhibit a gain of electrons after the adsorption event. Finally, these results provide important details in how the N-doping contributes to improving the interaction substantially with PbS nanoparticles, and these results suggest that when pyridine-like doping is present, the interaction is carried out by a Pb atom; however, on pristine SWCNTs, the main interaction is due to S atoms.

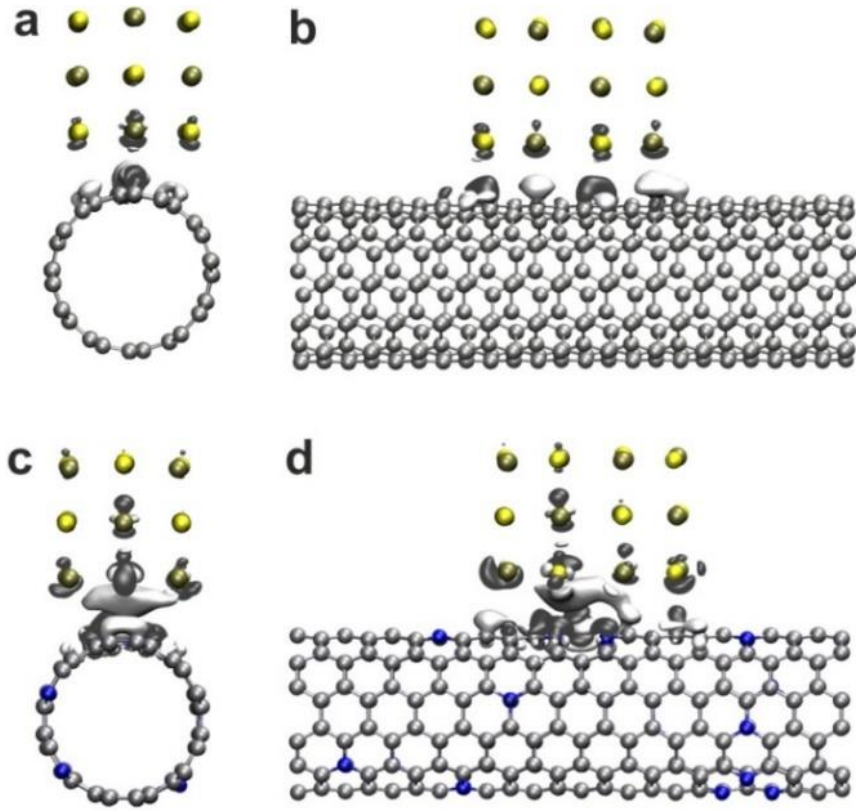

Figure 6. Optimized geometries and differences in charge density δn(r) of the $Pb_{18}S_{18}$ cluster adsorbed on (a-b) pristine (6,6)-SWCNT, and (c-d) a N-doped (6,6)-SWCNT. White color indicates areas with depletion of charge density after the $Pb_{18}S_{18}$ interaction. In contrast, black color illustrates areas where an increase in charge densities observed, the iso-surfaces value is plotted at ± 0.0005 $e^{-}Å^{-3}$. Yellow, gold, gray, and blue represent sulfur, lead, carbon, and nitrogen atoms, respectively.

4. Conclusions

PbS/N-CNTs composites were obtained by an environmentally friendly, simple, and inexpensive technique, where the PbS nanoparticles exhibited an average particle size of 15 nm with an FCC crystal structure. Raman spectroscopy, FT-IR, XRD, and SEM were used to identify the nature of the PbS/N-CNTs composites. FT-IR analysis shows the presence of C-S and S-S bonds within the PbS/N-CNTs composite, suggesting that organosulfur compounds might be protecting/passivating the PbS nanocrystals. Finally, *ab initio* theoretical calculations suggest that the nitrogenated sites along with the N-CNTs act as anchoring sites, where the interaction is carried out directly through the Pb atoms.

Acknowledgements

We thank Sergio Armando Roa Medina and Dafne E. Leyva-Tejeda for their collaboration, to the Tecnológico Nacional de México - Instituto Tecnológico Superior de Irapuato and the Benemérita Universidad Autónoma de Puebla for allowing us to use their facilities.

References

1. M. Terrones. *(*2004**).** Carbon nanotubes: synthesis and properties, electronic devices and other emerging applications. *Int. Mater. Rev*, 49, 325-377, https://doi.org/10.1179/174328004X5655
2. M. Terrones, P.M. Ajayan, F. Banhart, X. Blase, D.L. Carroll, J.C. Charlier, R. Czerw, B. Foley, N. Grobert, R. Kamalakaran, P. Kohler-Redlich, M. Rühle, T. Seeger, H. Terrones. *(*2002**).** N-doping and coalescence of carbon nanotubes: synthesis and electronic properties. *Appl. Phys. A* 74, 355-361, https://doi.org/10.1007/s003390201278
3. C.P. Ewels, M. Glerup. **(**2005**).** Nitrogen doping in carbon nanotubes. *J. Nanosci. Nanotechnol*, 5, 1345-1363, https://doi.org/10.1166/jnn.2005.304
4. X. Sun, R.Q. Yu, G.Q. Xu, T.S.A. Hor, W. Ji. (1998). Broadband optical limiting with multiwalled carbon nanotubes. *Appl. Phys. Lett.*, 73, 3632-3634, https://doi.org/10.1063/1.122845
5. P. Ayala, A. Grünesis, C. Kramberger, M.H. Rümmeli, I.G. Solórzano, F.L. Freire, T. Pichler. (2007). Effects of the reaction atmosphere composition on the synthesis of single and multiwalled nitrogen-doped nanotubes. *J. Chem. Phys*., 127, 184709, https://doi.org/10.1063/1.2781509
6. Z. Sun, Z. Liu, J. Li, G. Tai, S.P. Lau, F. Yan. (2012). Infrared photodetectors based on CVD-grown graphene and PbS quantum dots with ultrahigh responsivity. *Adv.Mater*., 24, 5878-5883, https://doi.org/10.1002/adma.201202220
7. Z.J. Zhou, G.T. Yu, F. Ma, X.R. Huang, Z.J. Wu, Z.R. Li. (2014). Theoretical investigation on nonlinear optical properties of carbon nanotubes with Stone–Wales defect rings. *J. Mater. Chem. C*, 2, 306-311, https://doi.org/10.1039/C3TC31904K
8. T.F. Kuo, C.C. Chi, I.N. Lin. (2001). Synthesis of carbon nanotubes by laser ablation of graphites at room temperature. *Jpn. J. Appl. Phys*., 40, 7147-7150, https://doi.org/10.1143/JJAP.40.7147
9. G.Z. Chen, D.J. Fray. (2003). Recent development in electrolytic formation of carbon nanotubes in molten salts. *J. Min. Metall.*, 39, 309-342, https://doi.org/10.2298/JMMB0302309C
10. Z. Xiong, Y.S. Yun, H.J. Jin. (2013). Applications of carbon nanotubes for lithium ion battery anodes. *Materials*, 6, 1138-1158, https://doi.org/10.3390/ma6031138
11. M. Terrones. (2003). Science and technology of the twenty-first century: synthesis, properties, and applications of carbon nanotubes. *Annu. Rev. Mater. Sci.*, 33, 419-501, https://doi.org/10.1146/annurev.matsci.33.012802.100255
12. O. Portillo Moreno, R. Gutiérrez Pérez, R. Palomino Merino, M. Chávez Portillo, G. Hernández Téllez, E. Rubio Rosas. (2016). Optical and structural properties of $PbSIn^{3+}$ nanocrystals grown by chemical bath. *Thin Solid Films*, 616, 800-807, https://doi.org/10.1016/j.tsf.2016.10.018
13. O. Portillo Moreno, R. Gutiérrez Pérez, M. Chávez Portillo, G. Hernández Téllez, E. Rubio Rosas, S. Cruz Cruz, A. Moreno Rodríguez. (2016). Synthesis, morphological, optical and structuralproperties of $PbSSe^{2-}$nanocrystals. *Optik*, 127, 8341-8349, https://doi.org/10.1016/j.ijleo.2016.06.022
14. W. Feng, C. Qin, Y. Li, W. Lwo, H. An, Y. Feng. (2014). A layer nanostructured assembly of PbS quantum dot/multiwalled carbon nanotube for a high performance photoswitch. *Sci. Rep*, 3777. 1, https://doi.org/10.1038/srep03777

15. A. Das, E. Hall, C.M. Wai. (2014). Noncovalent attachment of Pbs quantum dots to single and multiwalled carbon nanotubes. *J. Nanotech*, 1155, 285857.https://doi.org/10.1155/2014/285857
16. S. Jana, D. Banerjee, A. Jha, K.K. Chattopadhyay. (2011). Fabrication of PbS nanoparticle coated amorphous carbon nanotubes: Structural, thermal and field emission properties. *Mat. Res. Bull*., 46, 1659-1664, https://doi.org/10.1016/j.materresbull.2011.06.006
17. C.V.V.M. Gopi, S. Ravi, S.S. Rao, A.E. Reddy, H.J. Kim. (2017). Carbon nanotube/metal-sulfide composite flexible electrodes for high-performance quantum dot-sensitized solar cells and supercapacitors. *Sci.Rep.*, 46519 1, https://doi.org/10.1038/srep46519
18. F. Tuinstra, J.L. Koenig. (1970). Raman spectrum of graphite, *J. Chem. Phys*., 53, 1126, https://doi.org/10.1063/1.1674108
19. J. Maultzsch, S. Reich, C. Thomsen. (2007). Raman Scattering in Carbon Nanotubes. *Phys. Rev. B* 65 233402, https://doi.org/10.1103/PhysRevB.65.233402
20. M.S. Dresselhaus, G. Dresselhaus, R. Saito, A. Jorio. (2005). Raman spectroscopy of carbon nanotubes. *Phys.Rep*., 409, 47-99, https://doi.org/10.1016/j.physrep.2004.10.006
21. M. Chávez Portillo, X. Mathew, H. Juárez-Santiesteban, M. Pacio Castillo, O. Portillo Moreno. (2016). Growth and characterization of nanocrystalline PbS:Li thin films. *Superlattices Microstruct*, 98, 242-252, https://doi.org/10.1016/j.spmi.2016.08.032
22. R. Gutiérrez Pérez, O. Portillo Moreno, R. Palomino Merino, L.A. Chaltel Lima, M.N. Márquez Specia, G. Hernández Téllez, E. Rubio Rosas, A. Moreno Rodríguez. (2018). Optical, morphological and structural characterization of Er^{3+}-Bi^{3+} co-doped PbS nanocrystals grown by chemical bath. *Optik*, 162, 182-195. https://doi.org/10.1016/j.ijleo.2018.02.077
23. N. Perea-López, B. Rebollo-Plata, J.A. Briones-León, A. Morelos-Gómez, D. Hernández-Cruz, G.A. Hirata, V. Meunier, A.R. Botello-Méndez, J.C. Charlier, B. Maruyama, E. Muñóz-Sandoval, F. López-Urías, M. Terrones, H. Terrones. (2011). Millimeter-long carbon nanotubes: outstanding electron-emitting sources. *ACS Nano*, 5, 5072-5077, https://doi.org/10.1021/nn201149y
24. E. Gracia-Espino, B. Rebollo-Plata, H. Martínez-Gutiérrez, E. Muñoz-Sandoval, F. López-Urías, M. Endo, H. Terrones, M. Terrones. (2016). Temperature dependence of sensors based on silver-decorated nitrogen-doped multiwalled carbon nanotubes. *J. Sens*., 10, 4319498, https://doi.org/10.1155/2016/4319498
25. A. Lobo Guerrero, B. Rebollo-Plata, J.H. García Gallegos, D. Bahena Uribe, M.A. Guzmán Altamirano, J-G. Cabal-Velarde. (2021). Study of bamboo-type carbon nanotubes with magnetic iron carbide nanoparticles fabricated by a modified CVD method. *J. Nanopart. Res*., 23:94. https://doi.org/10.1007/s11051-021-05207-3
26. B. Hammer, L.B. Hansen, J,K, Nørskov. (1999). Improved adsorption energetics within density-functional theory using revised Perdew-Burke-Ernzerhoffunctionals. *Phys. Rev. B*, 59, 7413-7421, https://doi.org/10.1103/PhysRevB.59.7413
27. N. Troullier, J.L. Martins. (1991). Efficient pseudopotentials for plane-wave calculations. *Phys. Rev. B*, 43, 1993-2006, https://doi.org/10.1103/PhysRevB.43.1993
28. J.M. Soler, E. Artacho, J.D. Gale, A. García, J. Junquera, P. Ordejón, D. Sánchez-Portal. (2002). The SIESTA method for ab initio order-N materials simulation. *J. Phys.: Condens. Matter*, 14, 2745-2779, https://doi.org/10.1088/0953-8984/14/11/302
29. F.M. Bickelhaupt, N.J.R. van Eikema Hommes, C.F. Guerra, E.J. Baerends. (1996). The carbon−lithium electron pair bond in $(CH_3Li)_n$ (n = 1, 2, 4). *Organometallics*, 15, 2923-2931, https://doi.org/10.1021/om950966x
30. F. Villalpando-Paez, A. Zamudio, A.L. Elias, H. Son, E.B. Barros, S.G. Chou, Y.A. Kim, H. Muramatsu, T. Hayashi, J. Kong, H. Terrones, G. Dresselhaus, M. Endo, M. Terrones, M.S. Dresselhaus. (2006). Synthesis and characterization of long strands of nitrogen-doped single-

walled carbon nanotubes. *Chem. Phys. Lett.*, 424, 345-352, https://doi.org/10.1016/j.cplett.2006.04.074

31. A. Phuruangrat, T. Thongtem, S. Thongtem. (2011). Characterization and photo-luminescence of PbS nanocubes synthesized by a solvothermal method. *Chalcogenide Lett.*, 8, 297-300.
32. N. Choudhury, B.K. Sarma. (2009). Structural characterization of lead sulfide thin films by means of X-ray line profile analysis. *Bull. Mater. Sci.*, 32, 43-47, https://doi.org/10.1007/s12034-009-0007-y
33. M. Endo, Y.A. Kim, Y. Fukai, T. Hayashi, M. Terrones, H. Terrones, M.S. Dresselhaus. (2001). Comparison study of semi-crystalline and highly crystalline multiwalled carbon nanotubes. *Appl. Phys. Lett.*, 79, 1531-1533, https://doi.org/10.1063/1.1400774
34. A.P. Gaiduk, P.I. Gaiduk, A.N. Larsen. (2008). Chemical bath deposition of PbS nanocrystals: Effect of substrate. *Thin Solid Films*, 516, 3791-3795, https://doi.org/10.1016/j.tsf.2007.06.122
35. K. Stadelmann, A. Elizabeth, N.M. Sabanés, K.F. Domke. (2017). The SERS signature of PbS quantum dot oxidation. *Vib. Spectrosc*, 91, 157-162, https://doi.org/10.1016/j.vibspec.2016.08.008
36. S. Xiong, B. Xi, D. Xu, C. Wang, X. Feng, H. Zhou, Y. Qian. (2007). L-Cysteine-Assisted Tunable Synthesis of PbS of Various Morphologies. *J. Phys. Chem. C*, 111, 16761-16767, https://doi.org/10.1021/jp075096z
37. C. Thomsen, S. Reich. (2007). Raman Scattering in Carbon Nanotubes. In M. Cardona, R. Merlin (Eds.), Light Scattering in Solid IX. *Topics in Applied Physics*, Volume 108, pp. 115-232, 978-3-540-34436-0
38. T.Ch. Hirschmann, M.S. Dresselhaus, H. Muramatsu, M. Seifert, U. Wurstbauer, E. Parzinger, K. Nielsch, Y.A. Kim, P.T. Araujo. (2015). G' band in double- and triple-walled carbon nanotubes: A Raman study. *Phys. Rev. B*, 91 075402, https://doi.org/10.1103/PhysRevB.91.075402
39. S. Berciaud, S. Ryu, L.E. Brus, T.F. Heinz. (2009). Probing the Intrinsic Properties of Exfoliated Graphene: Raman Spectroscopy of Free-Standing Monolayers. *Nano Lett.*, 9, 346-352, https://doi.org/10.1021/nl8031444
40. A.O. Osikoya, D. Wankasi, R.M.K. Vala, C.W. Dikio, A.O. Afolabi, N. Ayawei, E.D. Dikio. (2015). Synthesis, characterization and sorption studies of nitrogen-doped carbon nanotubes. *Digest journal of Nanomaterials and Biostructures*, 10, 125-134.
41. J. Coates. (2006). Interpretation of Infrared Spectra, A Practical Approach. In M.A. Meyers, M.L. McKelvy, (Eds), *Encyclopedia of Analytical Chemistry*, John Wiley & Sons, https://doi.org/10.1002/9780470027318.a5606
42. W. Feng, C. Qin, Y. Shen, Y. Li, W. Luo, H. An, Y. Feng. (2014). A layer-nanostructured assembly of PbS quantum dot/multiwalled carbon nanotube for a high-performance photoswitch. *Sci. Rep.*, 4, 3777, https://doi.org/10.1038/srep03777